IEEE Access
Multidisciplinary | Rapid Review | Open Access Journal

Received September 15, 2021, accepted September 25, 2021, date of publication October 11, 2021,
date of current version January 13, 2022.

Digital Object Identifier 10.1109/ACCESS.2021.3117693

1-Bit Wideband Reconfigurable Reflectarray Design in Ku-Band

BIN XI[1], YU XIAO[1], (Member, IEEE), KAIQIANG ZHU[2], YOUWEI LIU[3], HOUJUN SUN[2], AND ZENGPING CHEN[1]

[1]School of Electronics and Communication Engineering, Sun Yat-sen University, Shenzhen 518104, China
[2]Beijing Key Laboratory of Millimeter-Wave and Terahertz Wave Technology, Beijing Institute of Technology, Beijing 100081, China
[3]54th Research Institute of CETC, Shijiazhuang 050299, China

Corresponding author: Yu Xiao (xiaoy283@mail.sysu.edu.cn)

This work was supported by the Natural Science Foundation of China under Grant 62001522.

ABSTRACT In this paper, a 1-bit wideband electronically reconfigurable reflectarray (RRA) in Ku-band is proposed. In order to achieve the wideband and reconfigurable characteristics, the stacked microstrip structure and a 1-bit ''microstrip line-slot line-microstrip line'' phase shifter (MSMPS) were introduced in this design. A novel ''receiving-phase shift-transmitting'' unit cell was gotten by connecting two stacked microstrip structures using MSMPS. Due to the receiving and transmitting parts are perpendicular to each other, the polarization rotation characteristic was demonstrated. To avoid the blockage of the feed horn, it was placed above the reflecting surface array with an offset angle of 25° to the normal direction. A 16 × 16 obliquely-fed RRA was designed and fabricated. The measured 1-dB gain bandwidth of the RRA is 15.4%. The measured results show that the fabricated prototype can achieve beam scanning from −20° to 50° in the elevation plane, and ±50° beam scanning in the azimuth plane.

INDEX TERMS Beam-scanning, PIN diodes, reconfigurable, polarization rotation, wideband, reflectarray.

I. INTRODUCTION

Antennas with wideband and beam-scanning characteristics are critically essential in many applications, such as wireless communication, remote sensing and so on. The phased array is a classical structure to achieve the beam-scanning capacity [1]. The beam scanning is achieved by manipulating the phase shifting of every phase shifter, which is connected to the antenna element [2]. However, due to the bulky and high cost of the phase shifter, the phased array is inconvenient in actual applications [3].

Recently, reconfigurable reflectarray antennas (RRAs) with various functions have been widely used due to they combine the features of reflectors and phased arrays [4]–[14]. The beam-scanning characteristics can be achieved by mechanically [4]–[7] or electronically [8]–[14] controlling phased responses of each element in RRA.

For mechanically controlling [4], the beam scanning is generally achieved by the rotation of the array, the rotation of the feed horn, or combines the two mentioned approaches. In [5], the proposed RA antenna achieves a beam scanning range of more than ±60° based on the mechanical rotation of the array. In [6], a wide-angle beam-scanning RA based on the mechanical rotation of the feed antenna was proposed, and the gain variation was less than 1.7 dB within the scan coverage of ±45°. In [7], a low-cost 1-D RRA with ±70° scan coverage was introduced by combining feed displacement and reflectarray panel in-plane rotation. All these works have been proved to be effective in realizing beam-scanning. However, the rotation of the array or feed antenna increases the complexity of the RRA application.

Phase response of electronically reconfigurable elements can be realized by PIN diodes [8], varactor diodes [9] and microelectromechanical systems (MEMS) switches [10]. Due to the continuous phase shift with a low transmission loss is fairly difficult and the control board is complex [11], PIN diodes are more commonly used in research [12]. The concept of phase quantization is widely used in RRA design. Among them, the 1-bit phase quantization design is a typical representation, that is, 0° and 180° states are used to substitute the continuous phase changes [13]. In [14], a wideband 1-bit 12 × 12 RRA was designed based on PIN diodes, and beam scanning within ±50° could be achieved in two principal planes. In [15], an X-band electronically RRA was

The associate editor coordinating the review of this manuscript and approving it for publication was Kai-Da Xu.

developed, and good beam-scanning performance has been achieved in a 2D space. In [16], an electronically reconfigurable folded reflectarray based on PIN diodes was proposed. The measurements of the fabricated prototype show a wide beam-scanning range up to ±60°. All these proposed electronically-controlled RRAs show a good beam-scanning characteristic.

A 1-bit electronically RRA with wideband, beam-scanning, and polarization rotation characteristics in Ku-band is proposed in this paper. A novel "receiving-phase shift-transmitting" reflecting element is established by connecting two stacked microstrip structures using a "microstrip line-slot line-microstrip line" phase shifter (MSMPS). The 1-bit reconfigurable characteristic is realized by two reversely-mounted PIN diodes on the MSMPS. Due to the receiving and transmitting parts are perpendicular to each other, the polarization rotation characteristic is gotten. The stacked structure design [17] is introduced to broaden the bandwidth, and a large polarization rotation bandwidth (over 20%) has been demonstrated. An RRA prototype is fabricated and measured. The measured beam can scan from −20° to 50° in the elevation plane, and ±50° beam scanning in the azimuth plane.

This paper is organized as follows. In Section II, the design of the 1-bit RRA unit cell and its simulated performance is presented. In Section III, a 256-element RRA prototype is designed, fabricated, and measured to validate the design. Finally, conclusions are given in Section IV.

II. RECONFIGURABLE UNIT CELL DESIGN

To design a wideband RRA unit cell, a wideband stacked patch structure, and a 1-bit MSMPS were proposed. First, a stacked microstrip structure was introduced to realize the wideband characteristics. Then, a 1-bit MSMPS was designed based on the idea of current path reversal. At last, the 1-bit wideband reflectarray unit cell was realized and the direct current (DC) bias was designed.

A. WIDEBAND STACKED MICROSTRIP STRUCTURE

Generally, an RRA antenna consists of a planar array with reconfigurable elements and a feed for illuminate [15]. The receiving and transmitting parts of the RRA are designed on the planar array.

In order to achieve the wideband characteristic of the RA, a stacked microstrip patch structure with a parasitic patch, shown in Fig. 1, has been designed in this paper. It comprises three metallic layers (the ground plane, the driven patch, and the parasitic patch) and two substrates. Arlon AD 255C ($\varepsilon_{r1} = 2.55$, $\tan\delta = 0.0014$, and $h_1 = 1.58$ mm) and Arlon AD 1000 ($\varepsilon_{r2} = 10.2$, $\tan\delta = 0.0023$, and $h_2 = 0.635$ mm) are chosen as the upper substrate and lower substrate, respectively. There is no air gap between the upper and lower substrates. All the detailed structural dimensions of the stacked microstrip patch antenna are listed in Table 1.

The simulated reflection coefficient (S_{11}) and realized gain of the wideband stacked microstrip patch antenna can be obtained from Ansys HFSS with the radiation boundary condition, as shown in Fig. 2. The −10 dB impedance bandwidth of the stacked microstrip patch antenna is about 21.1% (from 11.22 GHz to 13.86 GHz). The simulated peak gain is 6.48 dB at 13.68 GHz, and the 1-dB gain drop bandwidth is 23.7% (from 11.17 GHz to 14.34 GHz).

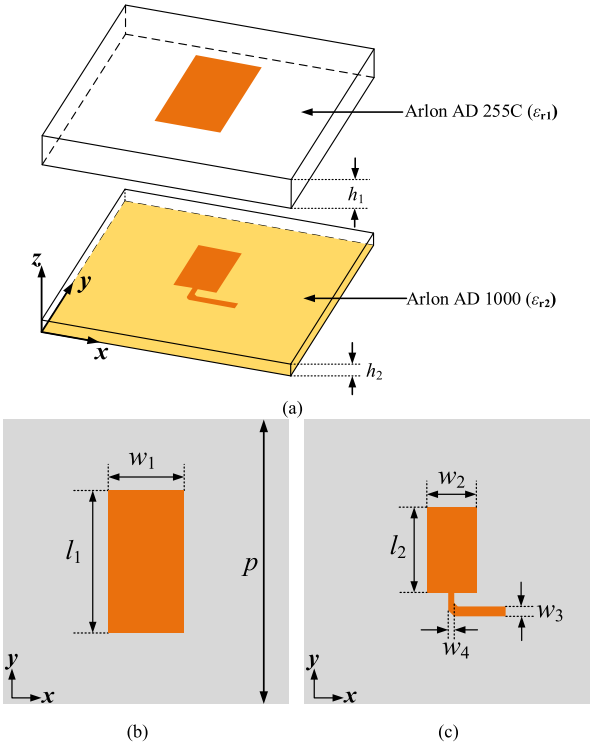

FIGURE 1. Structure of the stacked microstrip structure. (a) 3-D view; (b) Top view of the parasitic patch; (c) Top view of the driven patch.

TABLE 1. Parameters of the stacked microstrip structure.

Symbol	Size (mm)	Symbol	Size (mm)
p	12	w_3	0.4
w_1	3.2	w_4	0.24
l_1	6	h_1	1.58
w_2	2.1	h_2	0.635
l_2	3.6		

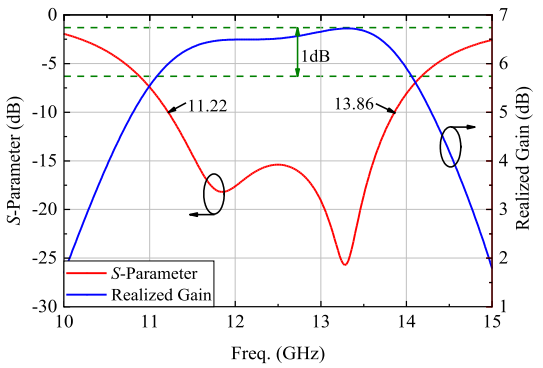

FIGURE 2. Simulated reflection coefficient and realized radiation gain of the stacked microstrip structure.

B. 1-BIT PHASE SHIFTER

In order to obtain the required 1-bit phase quantization (0° or 180°) and connect the receiving and transmitting parts simultaneously, a phase shifter is required. Based on the stacked microstrip structure design in Section II-A, an MSMPS [18], shown in Fig. 3, is designed. Here, Arlon AD 1000 ($\varepsilon_{r2} = 10.2$, $\tan\delta = 0.0023$, and $h_2 = 0.635$ mm) is selected to facilitate the connection of the receiving and transmitting parts. Port 1 and Port 2 are connected to microstrip line 1 and microstrip line 2, respectively. Meanwhile, another end of the microstrip line 1 is connected to the center of the inner circular metal patch (ICMP) at the bottom of the substrate by a metal via. The detailed parameters of the 1-bit MSMPS are listed in Table 2.

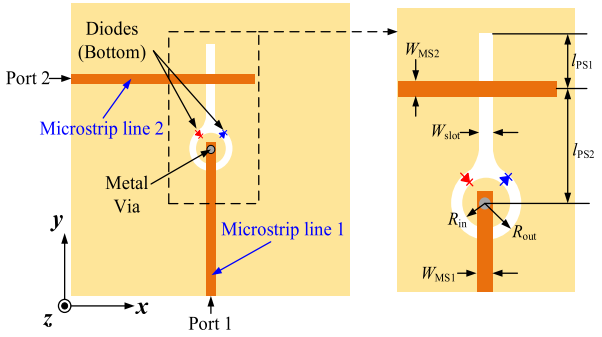

FIGURE 3. Structure of the MSMPS.

TABLE 2. Parameters of the MSMPS.

Symbol	Size (mm)	SYMBOL	Size (mm)
W_{MS1}	0.4	W_{slot}	0.35
W_{MS2}	0.4	R_{in}	0.65
l_{PS1}	1.37	R_{out}	0.95
l_{PS2}	2.9		

Two PIN diodes (MADP-000907-14020) are reversely mounted between the ground and the ICMP to obtain the required phase quantization [19]. By controlling the bias voltage, the working state of the diode will change and the path of the electromagnetic (EM) wave propagated in the slot will be changed accordingly. Fig. 4 shows the simulated electric field distributions of the MSMPS at 12.5 GHz under different states. Obviously, the propagation paths of the EM wave in State I and State II are opposite. Since the phase shift is achieved by changing the propagating path in a mirror direction, it can be called as "current path reversal principle."

To verify the characteristics of the MSMPS, the designed structure is simulated in *Ansys HFSS* with the radiation boundary condition. In simulations, the PIN diode is modeled as lumped elements. The initial value of the diode is $R = 7.8$ ohm and $L = 30$ pH in series for ON state, and $C = 0.025$ pF and $L = 30$ pH in series for OFF state [20]. Fig. 5 shows the simulated performance of the 1-bit MSMPS. The simulated results in State I and State II are basically the same. The minimum insertion losses of the MSMPS are

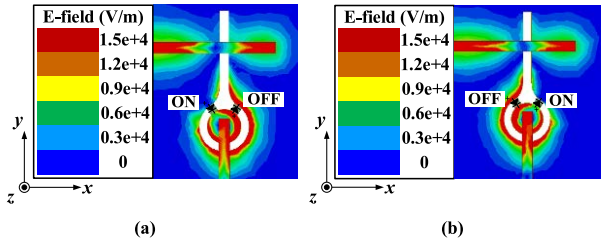

FIGURE 4. Electronic field distributions in different states. (a) State I; (b) State II.

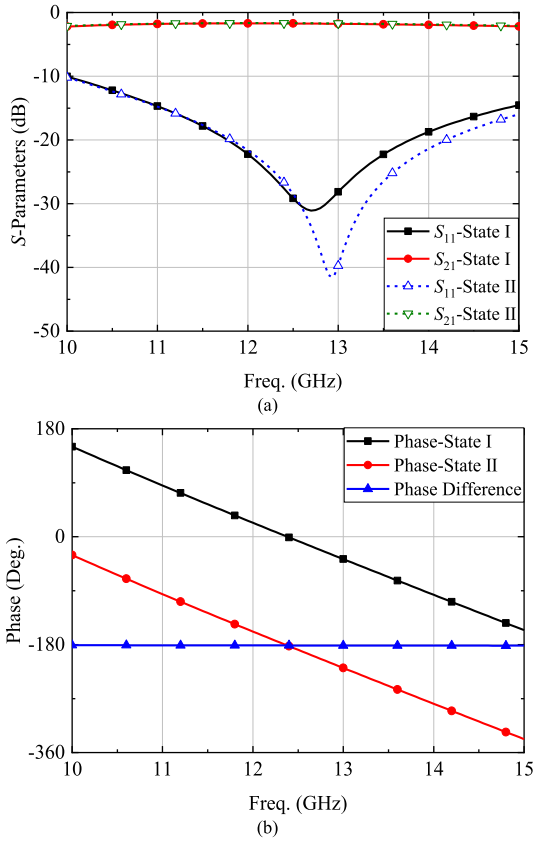

FIGURE 5. Simulated performances of the MSMPS. (a) S-parameters; (b) Phase.

1.7 dB for State I and 1.66 dB for State II. The simulated return losses in both states remain less than −10 dB in the operating band of 10∼15 GHz. The phase difference between State I and State II, shown in Fig. 5(b), remains around 180° within the operating band. The wideband characteristics of the 1-bit phase shifter are verified by the results.

C. REFLECTARRAY UNIT CELL AND BIAS NETWORK

A 1-bit RRA unit cell can be obtained by connecting the designed stacked microstrip patch structures in Section II-A using the MSMPS in Section II-B. Fig. 6 illustrates the structure of the proposed RRA unit cell. The top metal layer and the middle metal layer forms the stacked microstrip antennas, and the lower metal layer is the ground plane printed with the

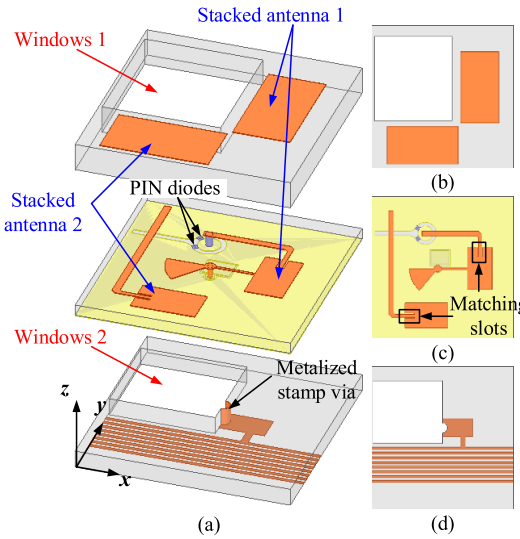

FIGURE 6. Structure of the proposed RRA unit cell. (a) Exploded view; (b) Top layer (Arlon AD 255C); (c) Middle layer (Arlon AD 1000); (d) DC bias layer (FR-4).

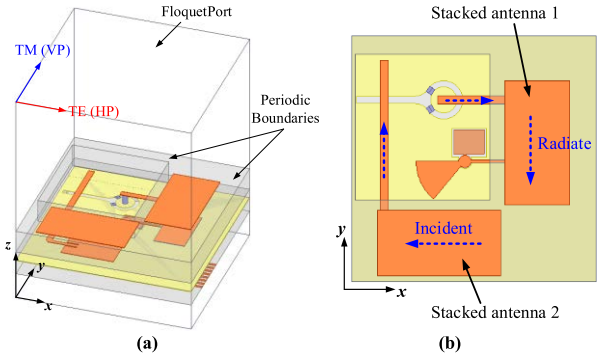

FIGURE 7. Full-wave simulated model and EM flow direction. (a) Full-wave simulated model; (b) EM flow direction.

slot line of the MSMPS (integrated with PIN diodes). The stacked antenna 1 and stacked antenna 2 are connected to microstrip line 1 and microstrip line 2 of the MSMPS (shown in Fig. 3), respectively. In order to achieve a better matching between the microstrip line and lower patch, two rectangular matching slots (0.2 mm × 0.8 mm, marked in Fig. 6(c)) are added at the connection. Besides, the part of the upper substrate with a size of 6.8 mm × 7.8 mm (windows 1 in Fig. 6) is cut off to avoid the effect of the upper substrate on MSMPS.

To control the diodes' states, a DC bias circuit is demanded for the RRA. Two conditions should be met for the DC bias network: RF signals should not enter the DC network, and DC signals should not interfere with the RF signals. As shown in Fig. 6(d), a DC bias board is placed under the ground of the unit cell. Here, the DC bias board is supported by FR-4 with a relative permittivity of 4.4 and a thickness of 1 mm. To realize the installation of the PIN diodes and avoid the effect of the lower substrate on MSMPS, a part of the FR-4 (windows 2 in Fig. 6) is cut off.

The bias lines are distributed on the back of the FR-4, and the DC bias voltage is added to the PIN diodes through the metalized stamp via. The DC bias voltage is applied to the middle of the lower patch of the stacked antenna 1 and transferred to the ICMP through the metal via to control the diode states. The bias line is a high-impedance microstrip line with a width of 0.2 mm, and a fan-shaped matching branch is added at about a quarter wavelength.

The characteristics of the RRA unit cell are analyzed with periodic boundary condition as shown in Fig. 7(a), and the periodic dimension is 12 mm × 12 mm (0.5 λ_0 × 0.5 λ_0, where λ_0 denote the free-space wavelength corresponding to 12.5 GHz). The Floquet port in *Ansys HFSS* is used to analyze the characteristics of the RRA unit cell. The TE and TM modes of the Floquet port are applied to calculate the horizontal polarization (HP) and vertical polarization (VP) incident waves, respectively. Here, we define the HP (TE mode) as along the x-axis, and the VP (TM mode) as along the y-axis. As shown in Fig. 7(b), when the EM wave is incident along the x-axis, it will be received by the stacked antenna 2. Then the EM wave will path through the MSMPS, and re-radiate along the y-axis by the stacked antenna 1. Conversely, the EM wave will be radiated by the stacked antenna 2 when it is received by the stacked antenna 1. Here, a typical "receive-phase shift-transmit" RRA structure is designed, and the polarization rotation characteristics are demonstrated.

The TE/TE means the reflected energy coming from the x-axis polarized wave (x-axis incident wave), and the TM/TE represents the reflected energy with the polarization rotating. The same definition also applies to the TM/TM and the TE/TM. Fig. 8(a) shows the simulated magnitude responses of the unit cell under TE mode and TM mode incidences (normal incidence and 30° oblique incidence are both contained). For normal incidence, the TM/TE (TE/TM) of the unit cell varies from 1.2 dB to 2.5 dB within the operating band of 11.6∼14.3 GHz. The fluctuation range of the TM/TE (TE/TM) is 1.0 dB within the operating band of 11.5∼14.3 GHz for 30° oblique incidence. Similarly, the TE/TE and TM/TM contained in Fig. 6(a) are basically less than −10 dB at the frequency range from 11.6 GHz to 14.3 GHz (corresponding to the relative bandwidth of 20.8%) for both the normal incidence and 30° oblique incidence.

Fig. 8(b) depicts the simulated phases and phase difference between the ON- and OFF-states for normal incidence. The simulated phase difference is maintained around 180° during the frequency band of 11.6 to 14.3 GHz. The wideband, oblique incidence and reconfigurable performances are demonstrated by the results.

A comparison between the simulated element performance of the proposed RRA element and some recently published RRA element designs is listed in Table 3. It is obvious that the proposed RRA element in this paper has advantages due to its wideband performance.

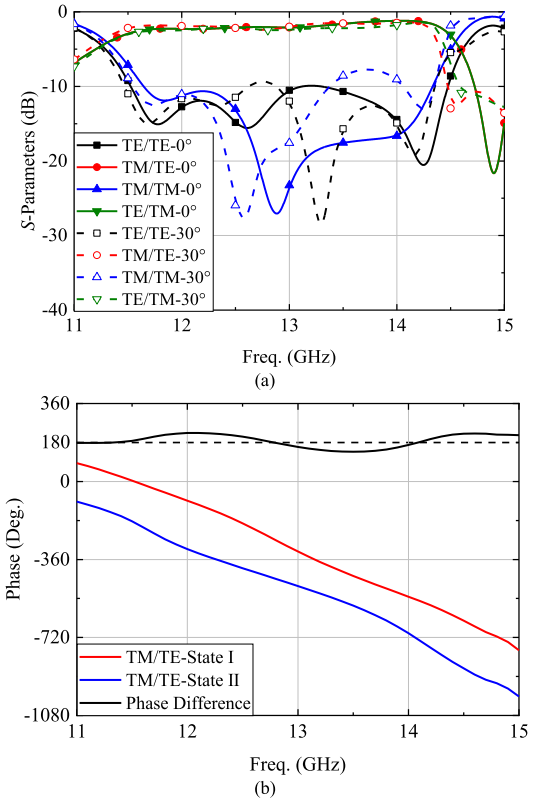

FIGURE 8. Simulated oblique incidence performance of the unit cell. (a) Magnitude responses; (b) Phase under normal incidence.

TABLE 3. Comparison of simulated performance of RRA elements.

Ref.	Freq. (GHz)	Phase control	Bandwidth (GHz)
[8]	12.5	PIN 1-bit	12.25~12.75 (4%)
[9]	5	Varactor Continuous	0.6%
[10]	11.2	MEMS 1-bit	12.5%
[12]	5	PIN 1-bit	4.7~5.3 (12%)
This work	**12.5**	**PIN 1-bit**	**11.6~14.3 (20.8%)**

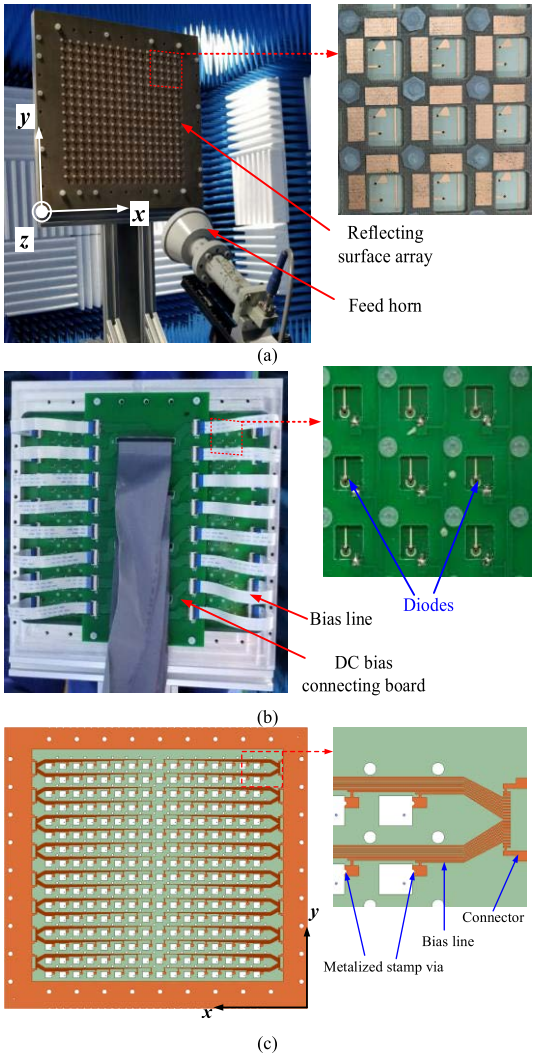

FIGURE 9. Photograph of the fabricated RRA. (a) Front view; (b) Back view; (c) Layout of biasing lines.

III. WIDEBAND RECONFIGURABLE REFLECTARRAY

A. CONFIGURATION OF THE REFLECTARRAY

Based on the proposed RRA unit cell in Section II-C, a 1-bit RRA with 16 × 16 elements, as shown in Fig. 9, was designed and fabricated. This RRA consists of a circular corrugated horn and a reflecting surface array. The aperture size of the reflectarray is 192 mm × 192 mm. In order to mitigate the blockage of the feed horn [16], an offset feed configurable is employed [21]. In this design, the feed horn is titled 25° away from the broadside direction. In order to control the fabricating cost here, the multi-layer structure connection of the reflecting array is achieved by a series of screws. For engineering production, different substrates can be pressed together by bonding film rather than screws.

A DC bias board is placed at the backside of the ground area. The layout of all DC bias lines is shown in Fig. 9(c). To control each RRA element independently, the 20-pin surface-mounted connector has been designed and used. The bias network includes 16 connectors, which are distributed on the right and left of the reflectarray. There are 256 bias lines in total, and each bias line starts from a connector and ends at different unit cells. All the bias lines in the bias board are connected on a connecting board and then connected to a 256-way voltage control board.

The focal length to diameter ratio (F/D) of the array is set to obtain a maximum aperture efficiency (the product of spillover efficiency and illumination efficiency). First, the performance of the feed horn is analyzed. Fig. 10(a) depicts the simulated reflection coefficient (S_{11}) and realized gain versus frequency of the horn. The simulated results show that the horn has a gain of 12.3∼15.9 dB within the frequency range of 11∼15 GHz, and S_{11} remains less than −20 dB. Radiation patterns of the E- and H-planes at 12.5 GHz are shown in Fig. 10(b). The radiation patterns of the E- and H- planes are in good agreement, and the E-/H-plane 3-dB beamwidth is 37.8°/35.4° at 12.5 GHz. Based on the radiation

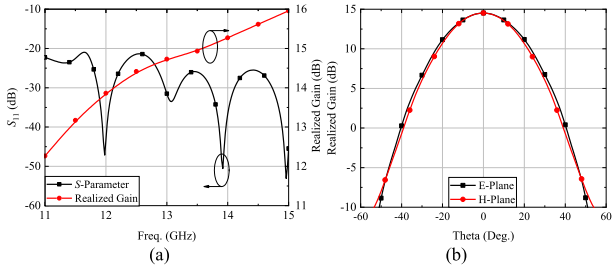

FIGURE 10. Simulated performance of the feed horn. (a) Reflection coefficient and realized gain versus frequency; (b) Radiation patterns at 12.5 GHz.

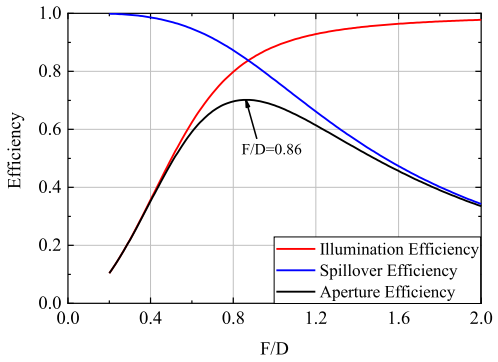

FIGURE 11. Calculated efficiency versus F/D. (Without considering the phase quantization error).

patterns of the horn, the effective Q factor is 5.5 in this design [22]. According to the geometry structure of the reflectarray, the calculated efficiency versus F/D is shown in Fig. 11. Here, the efficiency is calculated without considering the phase quantization error. The calculated maximum aperture efficiency is 70.2% when F/D is equal to 0.86, and the initial F/D of the RRA is set to be 0.86.

B. CONFIGURATION OF THE REFLECTARRAY

Based on the geometric parameters of the reflectarray, the required phase distribution for any beam direction can be calculated. Fig. 12 shows the side view of the reflectarray. The feed horn is placed above the reflecting surface array with an oblique angle of 25° to the normal direction, and point P refers to the phase center of the feed horn. Two elements A$(m, n, 0)$ and B$(p, q, 0)$ of the reflectarray are selected, where $(m, n, 0)$ and $(p, q, 0)$ express the coordinates of the element A and B, respectively.

To obtain a beam in a defined direction (such as $\boldsymbol{u_0}$ in Fig. 11), the EM waves reflected by elements should form an isophase plane perpendicular to $\boldsymbol{u_0}$, that is:

$$-k_0 d(m, n, 0) + \varphi_{req}(m, n, 0) + k_0 \vec{u}_0 \vec{r}_{mn} = -k_0 d(p, q, 0) + \varphi_{req}(p, q, 0) + k_0 \vec{u}_0 \vec{r}_{pq}, \quad (1)$$

where k_0 is the free space wavenumber corresponding to the required frequency (here, $f = 12.5$ GHz). $d(m, n, 0)$ and $d(p, q, 0)$ represent the distances from the center of element A and element B to the point F, respectively. $\boldsymbol{r_{mn}}$ and $\boldsymbol{r_{pq}}$ represent

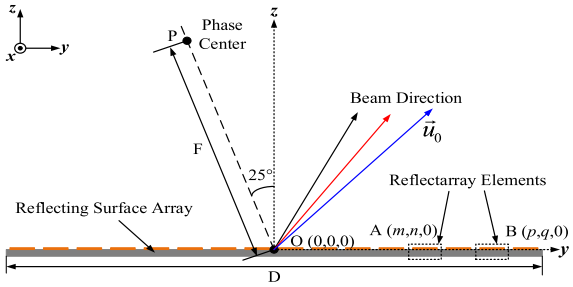

FIGURE 12. Side view of the RRA.

the position vectors of element A and element B, respectively. In addition, $\varphi_{\text{req}}(m, n, 0)$ and $\varphi_{\text{req}}(p, q, 0)$ mean the required phases of elements A and B, respectively, when the beam points to $\boldsymbol{u_0}$.

In order to obtain the required beam-scanning angle, the phase distributions on the 16 × 16 RRA elements for different directions are calculated. Fig. 13 shows the diode state distributions of RRA for the main beams of broadside direction and 30° oblique angles of the two principal planes. Due to the feed horn is distributed with an offset angle of 25° to the normal direction in the elevation plane (*yoz* plane), the beam-scanning is started from −20°. For the azimuth plane (*xoz* plane), the diode state distributions with the same offset angles (relative to the broadside) are symmetrical.

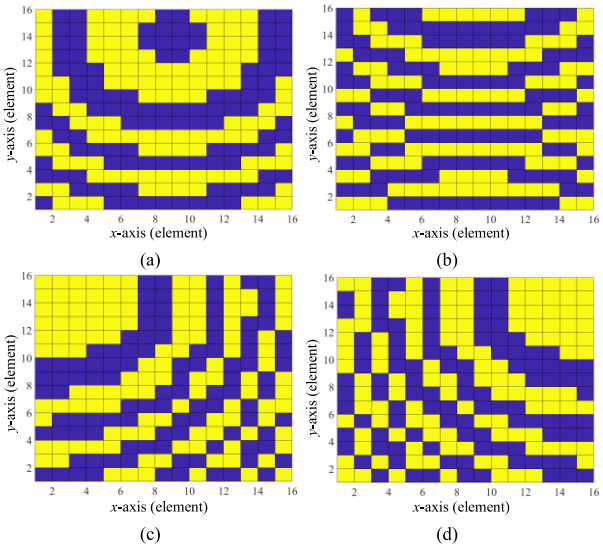

FIGURE 13. Diode state distributions of the RRA. (a) theta = 0°, phi = 0° (broadside); (b) theta = 30°, phi = 90° (*yoz* plane); (c) theta = −30°, phi = 0° (*xoz* plane); (d) theta = 30°, phi = 0° (*xoz* plane). ∗ denotes the OFF state; denotes the ON state.

C. SIMULATED AND MEASURED RESULTS

To demonstrate the design, the fabricated reflectarray prototype is measured in an anechoic chamber. Fig. 14 gives the simulated and measured realized gains of the reflectarray. The 1-dB gain drop bandwidth of the reflectarray is 15.4%

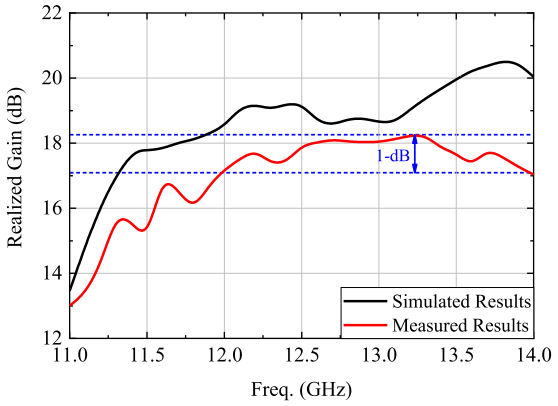

FIGURE 14. Simulated and measured realized gains versus frequency.

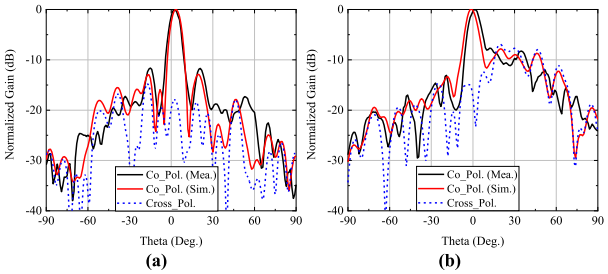

FIGURE 15. Simulated and measured radiation patterns of the broadside beams. (a) Azimuth plane (*xoz* plane); (b) Elevation plane (*yoz* plane).

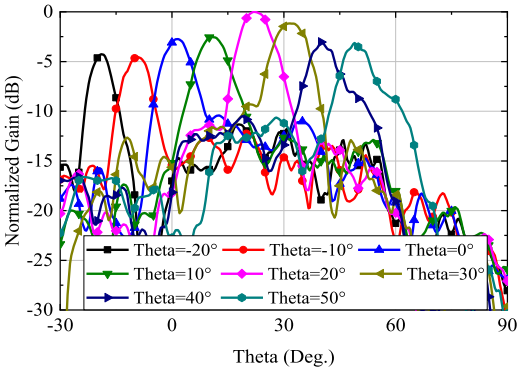

FIGURE 16. Measured radiation patterns in the elevation plane (*yoz*).

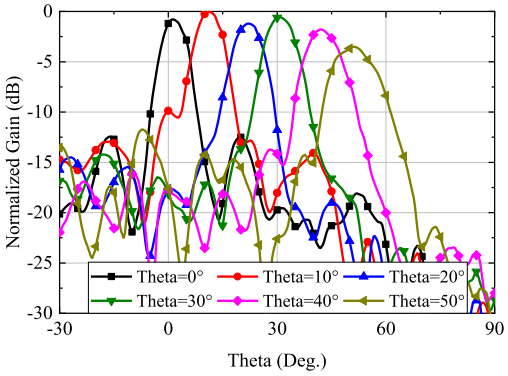

FIGURE 17. Measured radiation patterns in the azimuth plane (*xoz*).

(from 12 GHz to 14 GHz). The wideband characteristics of the proposed array are verified. The discrepancy between the simulated and measured results are may be attributed to the imperfect fabrication and soldering, and measurement accuracy. Besides, it is found that 20 PIN diodes are broken after assembly, which may cause an additional gain loss.

In the measurement, the EM wave emitted by the horn is linearly polarized along the *y*-axis direction, and the radiated EM wave is linearly polarized along the *x*-axis direction (as shown in Fig. 9). Conversely, it can also be used and the result is the same. The polarization rotation characteristics of the RRA are demonstrated.

The measured radiation patterns of the broadside beams at the two principal planes are shown in Fig. 15. To verify the feasibility, the simulated radiation patterns are also contained for comparison. Excellent agreements between the simulated and measured results are clearly observed in both the two principal planes. The measured half-power beam widths (HPBWs) are 8° and 8.7° in the azimuth and elevation planes, respectively. Besides, the cross-polarization levels are below −17.5 dB and −17 dB in the azimuth and elevation planes, respectively. The measured peak gain is about 20.5 dB, appearing at the 20° main beam, and the corresponding peak gain aperture efficiency is about 15.4%.

The beam-scanning performances in both the elevation plane (*yoz* plane) and azimuth plane (*xoz* plane) are measured at 12.5 GHz. Fig. 16 shows the measured radiation patterns in the elevation plane (*yoz* plane). Due to the feed horn is titled 25° away from the broadside direction in the elevation plane, the beam scanning is started from −20°. The measured results show that the proposed RRA can scan a range from −20° to 50° in the elevation plane, with a realized gain fluctuation of 4.5 dB.

Fig. 17 shows the measured radiation patterns of the RRA in the azimuth plane (*xoz* plane) at 12.5 GHz. The measured results show that the proposed RRA can scan a range from −50° to 50° with 3.5-dB gain fluctuation. Due to the symmetry in the azimuth plane, only the results of beam scanning from 0° to 50° are given in Fig. 17.

TABLE 4. Comparison of measured performance of RRAs.

Ref.	Freq. (GHz)	Mechanism	Number of elements	1-dB gain BW (%)	Aperture Eff. (%)	Scan range
[5]	26	Array rotation	20 × 20	13.1	/	±60° (1D)
[6]	12	Feed rotation	16 × 16	8~10	~ 43.1	±45° (1D)
[7]	12	Dual rotation	640	9.6	> 40	±70° (1D)
[8]	12.5	PIN	10 × 10	< 8	17.9	±50° (2D)
[14]	5	PIN	12 × 12	8.4	15.26	±50° (2D)
[15]	11.5	PIN	14 × 14	< 9	25.33	±60° (2D)
[16]	12.5	PIN	14 × 14	~ 12.5	13.2	±60° (2D)
This work	**12.5**	**PIN**	**16 × 16**	**15.4**	**15.4**	**±50° (2D)**

A comparison between the measured performances of the proposed RRA and some recent RRAs is listed in Table 4. It is worth mentioning that the presented RRA in this paper achieves the wider 1-dB gain drop bandwidth. Good polarization rotation characteristics have been gotten in this work. Besides, a comparable continuous beam-scanning performance has been achieved in contrast to previous works.

IV. CONCLUSION

In this paper, a 1-bit electronically controlled RRA with wideband, beam-scanning, and polarization rotation features in Ku-band was proposed. The unit cell consists of two stacked microstrip antennas and a 1-bit MSMPS. The wideband feature was realized by the stacked microstrip design, and the required phase quantization (0° and 180°) was obtained based on PIN diodes. The polarization rotation characteristic was demonstrated since the receiving and transmitting parts are perpendicular to each other. In order to mitigate the blockage of the feed horn, an offset feed configurable (titled 25° away from the broadside direction) was proposed. A 16 × 16 RRA was designed, fabricated, and measured. The fabricated prototype's main beam can scan from −20° to 50° in the elevation plane, and ±50° beam scanning in the azimuth plane.

REFERENCES

[1] C.-M. Liu, S.-Q. Xiao, H.-L. Tu, and Z. Ding, "Wide-angle scanning low profile phased array antenna based on a novel magnetic dipole," *IEEE Trans. Antennas Propag.*, vol. 65, no. 3, pp. 1151–1162, Mar. 2017.

[2] G. Yang, J. Li, S.-G. Zhou, and Y. Qi, "A wide-angle E-plane scanning linear array antenna with wide beam elements," *IEEE Antennas Wireless Propag. Lett.*, vol. 16, pp. 2923–2926, 2017.

[3] H. Yang, F. Yang, X. Cao, S. Xu, J. Gao, X. Chen, M. Li, and T. Li, "A 1600-element dual-frequency electronically reconfigurable reflectarray at X/Ku-band," *IEEE Trans. Antennas Propag.*, vol. 65, no. 6, pp. 3024–3032, Jun. 2017.

[4] P. Mei, S. Zhang, and G. F. Pedersen, "A low-cost, high-efficiency and full-metal reflectarray antenna with mechanically 2-D beam-steerable capabilities for 5G applications," *IEEE Trans. Antennas Propag.*, vol. 68, no. 10, pp. 6997–7006, Oct. 2020.

[5] M. I. Abbasi, M. H. Dahri, M. H. Jamaluddin, N. Seman, M. R. Kamarudin, and N. H. Sulaiman, "Millimeter wave beam steering reflectarray antenna based on mechanical rotation of array," *IEEE Access*, vol. 7, pp. 145685–145691, 2019.

[6] G.-B. Wu, S.-W. Qu, and S. Yang, "Wide-angle beam-scanning reflectarray with mechanical steering," *IEEE Trans. Antennas Propag.*, vol. 66, no. 1, pp. 172–181, Jan. 2018.

[7] G.-B. Wu, S.-W. Qu, S. Yang, and C. H. Chan, "Low-cost 1-D beam-steering reflectarray with ±70° scan coverage," *IEEE Trans. Antennas Propag.*, vol. 68, no. 6, pp. 5009–5014, Jun. 2020.

[8] H. Yang, F. Yang, S. Xu, Y. Mao, M. Li, X. Cao, and J. Gao, "A 1-bit 10 × 10 reconfigurable reflectarray antenna: Design, optimization, and experiment," *IEEE Trans. Antennas Propag.*, vol. 64, no. 6, pp. 2246–2254, Jun. 2016.

[9] L. Boccia, G. Amendola, and G. D. Massa, "Performance improvement for a varactor-loaded reflectarray element," *IEEE Trans. Antennas Propag.*, vol. 58, no. 2, pp. 585–589, Feb. 2010.

[10] T. Debogovic and J. Perruisseau-Carrier, "Low loss MEMS-reconfigurable 1-bit reflectarray cell with dual-linear polarization," *IEEE Trans. Antennas Propag.*, vol. 62, no. 10, pp. 5055–5060, Oct. 2014.

[11] S. V. Hum, M. Okoniewski, and R. J. Davies, "Modeling and design of electronically tunable reflectarrays," *IEEE Trans. Antennas Propag.*, vol. 55, no. 8, pp. 2200–2210, Aug. 2007.

[12] E. Carrasco, M. Barba, and J. A. Encinar, "X-band reflectarray antenna with switching-beam using PIN diodes and gathered elements," *IEEE Trans. Antennas Propag.*, vol. 60, no. 12, pp. 5700–5708, Dec. 2012.

[13] Y. Zhang, Z. Han, X. Lv, K. Yan, Z. Weng, and Z. Wu, "Novel one-bit digital coding broadband transmitarray antenna," *IEICE Electron. Exp.*, vol. 17, no. 13, Jul. 2020, Art. no. 20200195.

[14] J. Han, L. Li, G. Liu, Z. Wu, and Y. Shi, "A wideband 1 bit 12 × 12 reconfigurable beam-scanning reflectarray: Design, fabrication, and measurement," *IEEE Antennas Wireless Propag. Lett.*, vol. 18, no. 6, pp. 1268–1272, Jun. 2019.

[15] H. Zhang, X. Chen, Z. Wang, Y. Ge, and J. Pu, "A 1-bit electronically reconfigurable reflectarray antenna in X band," *IEEE Access*, vol. 7, pp. 66567–66575, 2019.

[16] Z. Wang, Y. Ge, J. Pu, X. Chen, G. Li, Y. Wang, K. Liu, H. Zhang, and Z. Chen, "1 bit electronically reconfigurable folded reflectarray antenna based on p-i-n diodes for wide-angle beam-scanning applications," *IEEE Trans. Antennas Propag.*, vol. 68, no. 9, pp. 6806–6810, Sep. 2020.

[17] A. Katyal and A. Basu, "Compact and broadband stacked microstrip patch antenna for target scanning applications," *IEEE Antennas Wireless Propag. Lett.*, vol. 16, pp. 381–384, 2017.

[18] Y. Xiao, B. Xi, M. Xiang, F. Yang, and Z. Chen, "1-bit wideband reconfigurable transmitarray unit cell based on PIN diodes in Ku-band," *IEEE Antennas Wireless Propag. Lett.*, early access, Jul. 27, 2021, doi: 10.1109/LAWP.2021.3100494.

[19] Y. Xiao, F. Yang, S. Xu, M. Li, K. Zhu, and H. Sun, "Design and implementation of a wideband 1-bit transmitarray based on a Yagi–Vivaldi unit cell," *IEEE Trans. Antennas Propag.*, vol. 69, no. 7, pp. 4229–4234, Jul. 2021.

[20] M. Wang, S. Xu, F. Yang, and M. Li, "Design and measurement of a 1-bit reconfigurable transmitarray with subwavelength H-shaped coupling slot elements," *IEEE Trans. Antennas Propag.*, vol. 67, no. 5, pp. 3500–3504, May 2019.

[21] X. Yang, S. Xu, F. Yang, M. Li, Y. Hou, S. Jiang, and L. Liu, "A broadband high-efficiency reconfigurable reflectarray antenna using mechanically rotational elements," *IEEE Trans. Antennas Propag.*, vol. 65, no. 8, pp. 3959–3966, Aug. 2017.

[22] J. Huang, and J. A. Encinar, *Reflectarray Antennas*. Hoboken, NJ, USA: Wiley, 2007.

BIN XI was born in Shanxi, China, in 1993. He received the B.S. degree in communication engineering from Taiyuan University of Technology, Taiyuan, China, in 2016, and the M.S. degree in electronics and information engineering from Sun Yat-sen University, Guangzhou, China, in 2018, where he is currently pursuing the Ph.D. degree in electronics and communication engineering.

His current research interest includes phased array antenna design.

YU XIAO (Member, IEEE) received the B.S. degree in electronic engineering from the Communication University of China, Beijing, China, in 2011, and the M.S. and Ph.D. degrees in electrical engineering from Beijing Institute of Technology (BIT), Beijing, in 2013 and 2017, respectively. From 2017 to 2019, he was a Postdoctoral Researcher with the Department of Electronic Engineering, Tsinghua University, Beijing. In 2019, he joined the School of Electronics and Communication Engineering, Sun Yat-sen University, Guangzhou, China, as an Assistant Professor. His current research interests include novel designs of high-gain antennas for wideband and wide-angle applications, artificial electromagnetic (EM) structures, and millimeter-wave devices.

KAIQIANG ZHU was born in Shandong, China, in 1991. He received the B.S. degree in electronic and information engineering from Beijing Institute of Technology, Beijing, China, in 2014, where he is currently pursuing the Ph.D. degree in electromagnetic fields and microwave technology. His current research interests include terahertz systems and microwave circuit.

YOUWEI LIU was born in Hebei, China, in 1994. She received the M.S. degree in electronic and information engineering from Beijing Institute of Technology, Beijing, China, in 2019. She is currently working at the 54th Research Institute of CETC, Shijiazhuang, China. Her current research interest includes digital multi-beam communication systems.

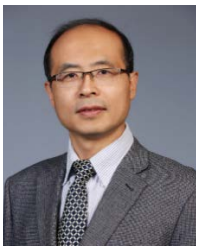

HOUJUN SUN received the Ph.D. degree in communication and electronic systems from Beijing Institute of Technology (BIT), in 1997. He is currently a Professor with BIT, the Director of the Institute of Microwave Technology, and the Director of Beijing Key Laboratory of Millimeter Wave and Terahertz Technology. His current research interests include integration and application of the millimeter-wave and terahertz communication systems, active antenna arrays, millimeter-wave imaging.

ZENGPING CHEN received the B.S. and Ph.D. degrees from the National University of Defense Technology, Changsha, China, in 1987 and 1994, respectively.

He is currently a Professor and a Ph.D. Supervisor with the School of Electronics and Communication Technology, Sun Yat-sen University. His current research interests include signal processing, radar systems, and automatic target recognition.